


Article

Surface Characteristics and Residual Stress Variation in Semi-Deep Hole Machining of Ti6Al4V ELI with Low-Frequency Vibration-Assisted Drilling

Joon-Hyeok Choe ¹ , Ju Hyung Ha ², Jisoo Kim ^{1,3,*} and Dong Min Kim ^{2,*}

¹ Department of Precision Mechanical Engineering, Kyungpook National University (KNU), Sangju-si 37224, Republic of Korea; choijh0424@knu.ac.kr

² Dongnam Division, Korea Institute of Industrial Technology (KITECH), Jinju-si 52845, Republic of Korea; hajh@kitech.re.kr

³ Department of Advanced Science and Technology Convergence, Kyungpook National University (KNU), Sangju-si 37224, Republic of Korea

* Correspondence: js.kim@knu.ac.kr (J.K.); dkm0707@kitech.re.kr (D.M.K.)

Abstract: This study examined the impact of vibration-assisted drilling (VAD) on hole quality and residual stress in Ti-6Al-4V ELI (Extra Low Interstitials) material. Ti-6Al-4V ELI possesses excellent mechanical properties but presents challenges in machining, including chip evacuation, burr formation, and elevated cutting temperatures. VAD, particularly low-frequency vibration-assisted drilling (LF-VAD), has been explored as a potential solution to address these issues. The research compares LF-VAD with conventional drilling (CD) under various cutting and cooling conditions. LF-VAD exhibits higher maximum thrust forces under specific conditions, which result in accelerated tool wear. However, it also demonstrates lower RMS (root mean square) forces compared to CD, offering better control over chip formation, reduced burr formation, and improved surface roughness within the hole. Furthermore, LF-VAD generates greater compressive residual stresses on the hole's inner surface compared to CD, suggesting enhanced fatigue performance. These findings indicate that LF-VAD holds promise for improving the hole's surface characteristics, fatigue life, and overall component durability in Ti-6Al-4V machining applications.

Keywords: Ti-6Al-4V ELI; machining; low-frequency vibration-assisted drilling; residual stress



Citation: Choe, J.-H.; Ha, J.H.; Kim, J.; Kim, D.M. Surface Characteristics and Residual Stress Variation in Semi-Deep Hole Machining of Ti6Al4V ELI with Low-Frequency Vibration-Assisted Drilling. *J. Manuf. Mater. Process.* **2023**, *7*, 209. <https://doi.org/10.3390/jmmp7060209>

Academic Editors: Alborz Shokrani and François Ducobu

Received: 13 October 2023

Revised: 22 November 2023

Accepted: 23 November 2023

Published: 27 November 2023



Copyright: © 2023 by the authors. Licensee MDPI, Basel, Switzerland. This article is an open access article distributed under the terms and conditions of the Creative Commons Attribution (CC BY) license (<https://creativecommons.org/licenses/by/4.0/>).

1. Introduction

Titanium alloys are renowned for their exceptional mechanical properties and are characterized by a high strength-to-weight ratio, inherent corrosion resistance, and outstanding fatigue and creep resistance [1,2]. These distinctive attributes have rendered titanium highly coveted in various high-value sectors, notably in aerospace and related industries [3]. Within this class of alloys, Ti-6Al-4V extra low interstitial (ELI) stands out for its notable suppression of impurities, resulting in enhanced ductility and fracture toughness compared with the conventional Ti-6Al-4V [4,5]. Notably, it maintains resilience even at extremely low temperatures, rendering it indispensable in cryogenic applications. Furthermore, this alloy finds extensive applications in diverse fields, including biomedical implants, aerospace components, and offshore equipment [6–8].

Despite these advantages, the machining of titanium-based alloys is recognized as a formidable challenge in the manufacturing industry. Common issues encountered include difficulties in chip removal, elevated cutting temperatures leading to tool welding, accelerated tool wear due to the material's low thermal conductivity, challenges in burr removal, and the material's high chemical affinity with tools [9–12]. These issues are exacerbated during drilling due to the enclosed machining environment, hindering heat and chip evacuation and resulting in elevated cutting temperatures and diminished surface

quality [13]. In particular, problematic chip evacuation generally leads to the formation of long, continuous chips that adversely impact surface quality, rendering drilling titanium alloys a complex task in real industrial settings [13]. To improve efficiency and productivity in machining titanium alloy holes, ongoing investigations explore various methods, including tool coatings [14,15], enhanced cooling processes [16,17], and innovative tool designs [18,19]. Vibration-assisted drilling (VAD) has emerged as a promising trend for addressing these challenges.

Vibration-assisted drilling (VAD) technology refers to the integration of axial tool vibration with conventional drilling (CD) to enhance cutting performance. It is categorized based on vibration frequency, with frequencies exceeding 20,000 Hz classified as ultrasonic vibration-assisted drilling (UVAD) [20,21]. If the frequency is generally above 1000 Hz, it is known as high-frequency vibration-assisted drilling (HF-VAD), and when it is below 1000 Hz, it is referred to as low-frequency vibration-assisted drilling (LF-VAD) [22–24]. Among these categories, LF-VAD stands out for its exceptional performance in chip generation and removal mechanisms. Research into chip-breaking phenomena in LF-VAD has been conducted for materials such as titanium alloys [25,26], titanium-CFRP composites [27–29], and aluminum [30], with both numerical and experimental studies exploring these phenomena.

However, existing research results mainly occupy cases where the hole depth is less than $2 \times D$ (hole diameter), and investigations into deeper holes are very limited [22,25,31]. Furthermore, previous research has mainly focused on dry machining and minimal quantity lubrication (MQL) for analyzing chip evacuation mechanisms. When deeper hole machining is required in the context of structural and mechanical components, dry or MQL cooling conditions are ineffective due to heat dissipation issues [32]. Therefore, powerful cooling conditions such as internal coolant are necessary. Additional research is needed to understand the impact of LF-VAD on such processing. Therefore, in this study, using Ti-6Al-4V ELI material, machining experiments are conducted at depths exceeding $2 \times D$ at various cooling conditions and cutting speeds. The research aims to provide suitable machining parameters for LF-VAD by analyzing thrust forces, tool wear, hole surface roughness, burr size, and residual stresses under different machining conditions.

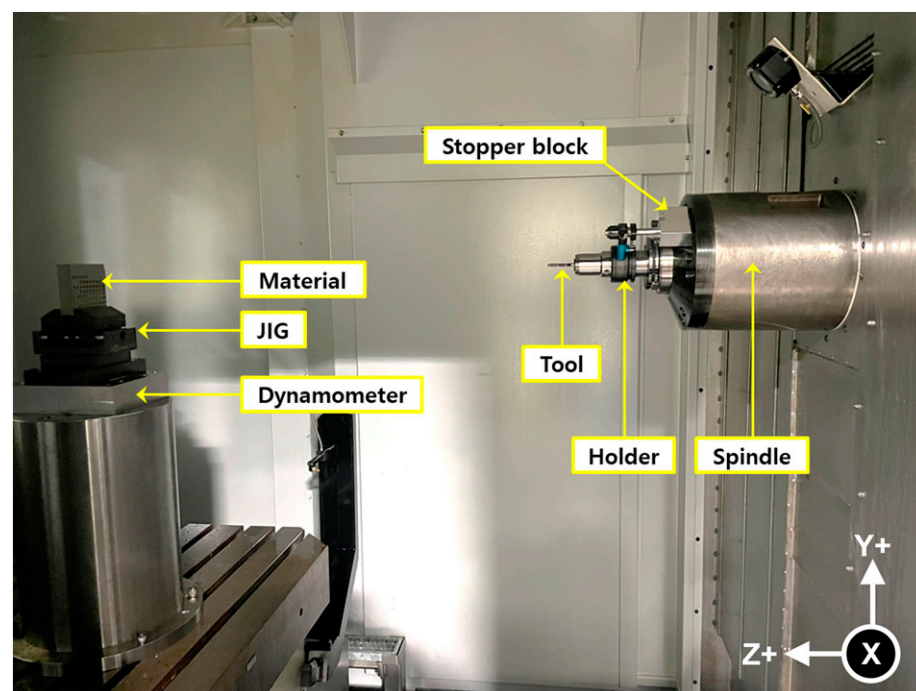
2. Materials and Methods

In this investigation, we employed the prevalent wet cooling method to examine variations in internal coolant pressure and cutting speed. To explore diverse conditions, we utilized two cutting fluid pressure levels (10 bar and 40 bar) along with three cutting speeds. These speeds encompassed the standard cutting speed of 40 m/s, commonly applied for stable cutting in industrial settings. Additionally, conditions of 80 m/s and 120 m/s were considered to assess distinctions in cutting behavior between LF-VAD machining in extreme environments and conventional drilling (CD). The selection of these conditions took into account the limitations of the LF-VAD holder (maximum RPM: 6500; maximum internal coolant pressure: 45 bar). The labeling and detailed machining conditions for each drilling condition are indicated in Table 1.

Figure 1 is a representation of the experimental setup. For CD machining, a 130 mm shrink fit holder (HAIMER) was employed, whereas MITIS's PM4225 holder was used for LF-VAD machining. The holder utilized in vibration-assisted drilling features a cam structure with a sinusoidal shape, generating 2.5 vibrations per revolution and an amplitude of 125 μm . The experiments were executed using a 4-axis DIXI JIG1200 boring machine center. All machining operations were conducted with a 9139AA dynamometer (KISTLER, Winterthur, Swiss) affixed to the jig base, capable of measuring thrust forces in the z -axis direction, aligning with the drilling direction per the equipment's reference. Collected data were recorded using a 5617A80 amplifier (KISTLER). In drilling operations, where cutting loads predominantly act in the tool's direction, cutting thrust in the drilling direction (z -axis) was measured. Forces recorded in the x and y -axis directions were not considered in the analysis.

Table 1. Detailed processing conditions according to each drilling label.

Label	Drilling Method	Cutting Speed [m/s]	Feed Rate [mm/min]	Coolant Pressure [bar]	Hole Depth [mm]
C-40-10	CD	40	169.77	10	30
C-40-40	CD	40	169.77	40	30
C-80-40	CD	80	339.54	40	30
C-120-10	CD	120	509.31	10	30
C-120-40	CD	120	509.31	40	30
L-40-10	LF-VAD	40	169.77	10	30
L-40-40	LF-VAD	40	169.77	40	30
L-80-40	LF-VAD	80	339.54	40	30
L-120-10	LF-VAD	120	509.31	10	30
L-120-40	LF-VAD	120	509.31	40	30

**Figure 1.** Experimental setup of DIXI JIG1200 boring machine center equipped with LF-VAD holder, tools, and dynamometer for processing and analyzing Ti-6Al-4V ELI.

The utilized tool possessed a standard diameter of 6 mm, a common size in the aerospace industry. Machining employed a TiAlN-coated WC drill (DREAM DRILL INOX DH452060, YG-1, Incheon, Korea). The Ti-6Al-4V ELI (Grade 23) titanium alloy blocks, with dimensions of 100 mm (W) × 100 mm (L) × 30 mm (H), served as the machining substrate. Table 2 provides details on the drill's specifications, while Table 3 outlines the physical and mechanical properties of the titanium alloy. For each set of conditions, 20 holes were machined, and chip collection occurred after the first and last holes were completed. The collected chips for analysis underwent resin mounting, grinding up to 2000 grit, and subsequent polishing down to 1 μ m. Following these steps, etching with Kroll's reagent for 10 s was conducted, followed by chip morphology and phase analysis. A few finished samples were cut at the hole center using electrical discharge machining (SL400G, SODICK, Yokohama, Japan) to measure surface roughness (SV-2100, Mitutoyo, Kawasaki, Japan) and residual stresses (μ -X360s, PULSTEC, Hamamatsu, Japan) within the hole. Surface roughness, assessed in terms of R_a values for an overall analysis of the hole's surface finish, was measured at different areas with 5 mm intervals, totaling five measurements. This process was repeated twice for each sample. Residual stress was measured on a central

area inside the hole with a diameter of 50 μm to minimize interference with the inner surface curvature of the hole, and the measurement was conducted for 120 s at the K-alpha wavelength. Thrust force, morphology of the chips, surface roughness, burr height, and residual stress are comprehensively reviewed to provide suitable processing conditions for LF-VAD processing.

Table 2. Specifications of the drill used in the experiments (DH452060, YG-1).

Coating Material	TiAlN
Diameter [mm]	6
Point Angle [°]	140
Helix Angle [°]	30
Cutting Length [mm]	44
Total Length [mm]	82

Table 3. Mechanical properties of the materials used in the experiments [33].

Mechanical Property	Ti-6Al-4V	Ti-6Al-4V ELI
Vickers Hardness	349	341
Tensile Strength, Ultimate [MPa]	950	860
Tensile Strength, Yield [MPa]	880	790
Modulus of Elasticity [GPa]	113.8	113.8
Charpy Impact [J]	17	24
Fracture Toughness [$\text{MPa}\cdot\text{m}^{1/2}$]	75	100
Reduction of Area [%]	36	15

3. Results

3.1. Thrust Force

Differences between LF-VAD and CD are initially compared through thrust forces, as presented in Table 4. LF-VAD is abbreviated as ‘L’ in experimental conditions, and CD is abbreviated as ‘C’ in experimental conditions. The experimental conditions mentioned below are labeled with cutting speed and coolant pressure information. For example, conventional drilling conditions using a cutting speed of 40 m/s and coolant pressure of 10 bar are expressed as ‘C-40-10’. This table shows the maximum and root mean square (RMS) thrust force values for various drilling methods and cutting conditions, along with labels for the experimental conditions. Figure 2 illustrates thrust force graphs for the L-40-40 and C-40-40 conditions, providing a visual representation of typical behavioral distinctions between the two cutting methods. As is evident in the graph, the thrust force in LF-VAD exhibits sinusoidal variation over time. To facilitate comparisons based on periodically changing values, RMS values were utilized for analysis instead of the mean value. Each RMS value was computed from a consistent intermediate segment of force variation (Vc40: 5 s, Vc80: 4 s, and Vc120: 2.5 s). This study conducted experiments under various conditions, encompassing different machining methods (CD and LF-VAD), diverse cutting speeds (40 m/s, 80 m/s, and 120 m/s), and varying cutting fluid pressures (10 bar and 40 bar). To systematically analyze these conditions, the thrust force analysis was divided into (1) maximum force and (2) RMS force analysis. The RMS force analysis section was further subdivided into (1) thrust force analysis based on cutting fluid pressure conditions and (2) thrust force analysis based on cutting speed.

Concerning maximum thrust force, LF-VAD conditions consistently recorded higher forces compared with CD, ranging from a decrease of 24% (L-40-40, 20 passes) to an increase of 133% (L-120-10, 20 passes). This phenomenon is attributed to the distinctive characteristics of the LF-VAD machining method. In contrast to the CD process, where a uniform depth (0.08 mm/rev in this study) is achieved at regular rotations, LF-VAD demonstrates continuously changing feed rates due to the sinusoidal vibration in the axial direction. Chips, which are cut to a consistent thickness in the CD process, become segmented in the LF-VAD process due to the applied vibration, inevitably resulting in

larger maximum forces [25]. This mechanism is schematically represented in Figures 2 and 3, and the schematic diagram of the chip generation mechanism in Figure 3 is based on the research results [29] of Haojun Yang et al.

Table 4. Thrust force trends by processing conditions and passes.

LF-VAD										
Test No.	L-40-10		L-40-40		L-80-40		L-120-10		L-120-40	
Cutting Speed; Vc [m/s]	40		40		80		120		120	
Coolant Pressure [bar]	10		40		40		10		40	
Pass	1	20	1	20	1	20	1	20	1	20
Maximum force [N]	976.29	1257.54	1116.38	1070.30	1200.81	1177.83	1189.29	1812.67	1202.10	1219.08
RMS force [N]	583.45	820.05	647.13	650.06	634.53	631.57	636.37	1044.70	581.39	572.21
CD										
Test No.	C-40-10		C-40-40		C-80-40		C-120-10		C-120-40	
Cutting Speed [m/s]	40		40		80		120		120	
Coolant Pressure [bar]	10		40		40		10		40	
Pass	1	20	1	20	1	20	1	20	1	20
Maximum force [N]	714.01	757.40	824.25	860.16	790.49	802.20	856.66	776.53	673.38	724.63
RMS force [N]	585.26	599.99	741.60	744.91	674.08	672.23	572.86	547.72	526.003	505.47

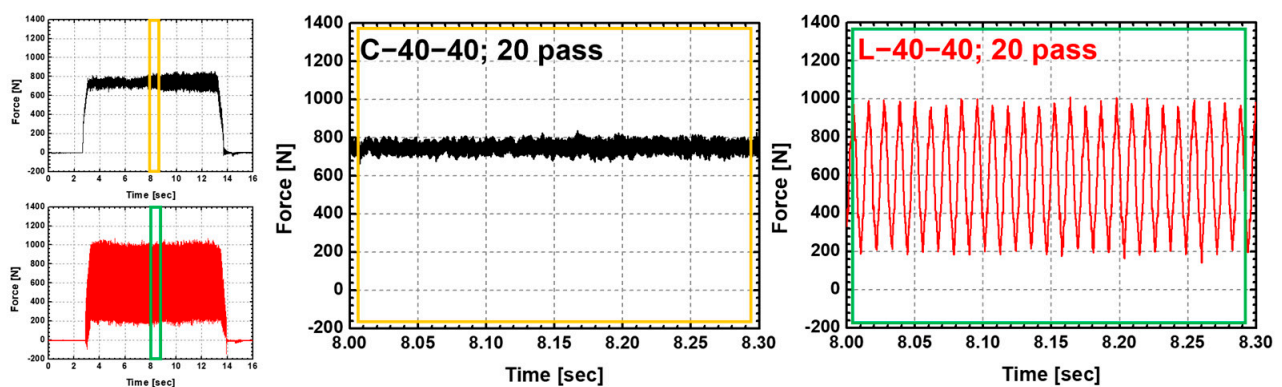


Figure 2. Comparison of thrust forces due to the difference in cutting methods between low-frequency vibration-assisted drilling (LF-VAD; abbreviated as ‘L’) and conventional drilling (CD; abbreviated as ‘C’) processes (Vc: 40 m/s, coolant pressure: 40 bar, 20 passes).

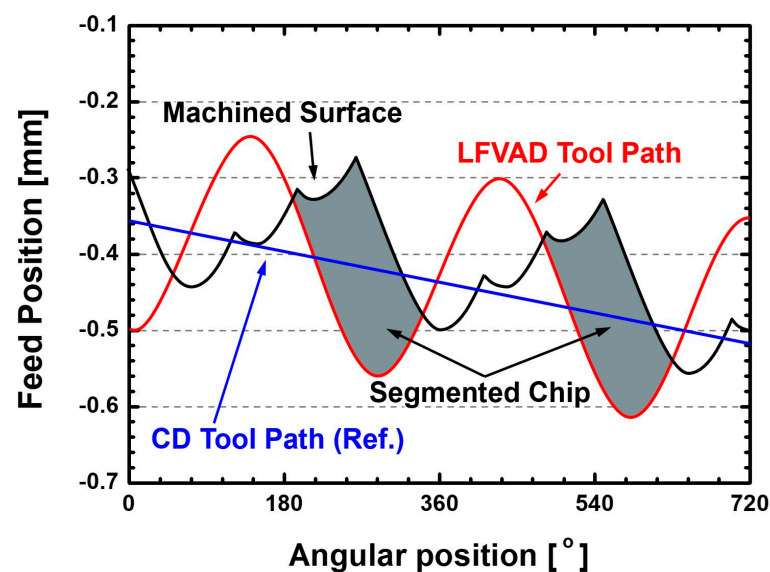


Figure 3. Schematic of the cutting process and chip formation mechanism in the LF-VAD process.

Maximum force represents the peak force applied to the tool at a specific moment, while RMS force indicates the continuous force acting on the tool during machining. In contrast to consistently higher maximum forces exhibited by LF-VAD compared to CD across all conditions, RMS values showed variations based on the cutting conditions.

Firstly, RMS values during hole machining varied depending on the cutting fluid pressure (10 bar and 40 bar). In CD, at a cutting speed of 40 m/s and over 20 passes, an increase in cutting fluid pressure resulted in a 24% increase in RMS force. However, at a cutting speed of 120 m/s, an increase in cutting fluid pressure led to a decrease of approximately 7% in RMS force. This highlights that higher cutting fluid pressure does not necessarily lead to improved thrust force in CD, emphasizing the need to adjust cutting fluid pressure based on cutting speed. CD exhibited a relatively stable trend in thrust force with increasing passes from 1 to 20 passes, irrespective of cutting fluid pressure. In LF-VAD conditions, changes in cutting fluid pressure led to a more pronounced impact. For instance, machining at a cutting speed of 120 m/s with a pressure of 10 bar (L-120-10) resulted in an increase in force from 636.37 N at 1 pass to 1044.70 N at 20 passes. Similarly, at a cutting speed of 40 m/s (L-40-10), forces measured were 578.45 N and 820.05 N at 1 pass and 20 passes, respectively. In contrast, under LF-VAD conditions with the same LF-VAD parameters but a cutting fluid pressure of 40 bar (L-40-40, L-80-40, and L-120-40), a minimal change in the thrust force was observed with increasing passes. This indicates that when the cutting fluid pressure is low at 10 bar, the increase in thrust force is significantly higher compared with machining at 40 bar. This observed phenomenon in LF-VAD machining conditions can be attributed to temperature during cutting. Basically, LF-VAD can promote the penetration of cutting fluid into the cutting zone, which alone can reduce friction in the machining area. However, low cutting fluid pressure (10 bar) in LF-VAD machining may not efficiently expel segmented chips, leading to increased cutting resistance. Additionally, in the LF-VAD process, where vibration occurs during processing and the material is processed at a higher feed rate, the degree of cooling may be worse compared to CD. Elevated cutting temperatures accelerate adhesion wear due to the high chemical affinity between titanium and the tool, promoting tool wear. Moreover, if these conditions persist and maintain high temperatures, they enhance material ductility, rendering it difficult for chips to segmentize. This hinders chip evacuation and increases cutting resistance, resulting in rapid tool wear.

Secondly, RMS force trends during hole machining varied with the cutting speed (40 m/s, 80 m/s, and 120 m/s). In CD, analyzing RMS force based on 1 pass revealed an order of thrust forces as follows: C-120-40 (526.00 N), C-120-10 (572.86 N), C-40-10 (585.26 N), C-80-40 (674.08 N), and C-40-40 (741.60 N), demonstrating an overall increase in the thrust force as the cutting speed decreases. This aligns with previous research indicating that as cutting speed increases (higher RPM and higher feed), cutting thrust force decreases. However, the trends exhibited variations according to the combination of cutting fluid pressure and cutting speed, underscoring the need for customized cutting conditions in CD machining situations. Under CD conditions, thrust forces from 1 pass to 20 passes exhibited a consistent trend across all conditions, with no significant increase in thrust force as the number of passes increased. Under LF-VAD conditions, similar to CD, the lowest thrust force was observed in the condition with the highest cutting speed, L-120-40. When comparing thrust forces for conditions machined with 40 bar of cutting fluid pressure (based on 1 pass), the order of thrust forces was L-120-40 (581.39 N), L-80-40 (634.53 N), and L-40-40 (647.13 N). Higher cutting speeds corresponded to lower thrust forces.

In conclusion, LF-VAD under all conditions exhibits a higher maximum thrust force compared to CD, and it is observed that RMS thrust values vary with coolant pressure. When machining with 40 bar pressure in LF-VAD, a lower RMS thrust force is observed compared to CD, while machining with 10 bar pressure tends to show an increasing trend.

3.2. Chip Extraction and Chip Formation

The chip shapes collected from the LF-VAD and CD machining processes after 20 passes are depicted in Figure 4. In LF-VAD, axial vibration is introduced to the axial feeding movement of the CD process. This sinusoidal vibration effectively segments the chips, facilitating their crushing and subsequent removal.

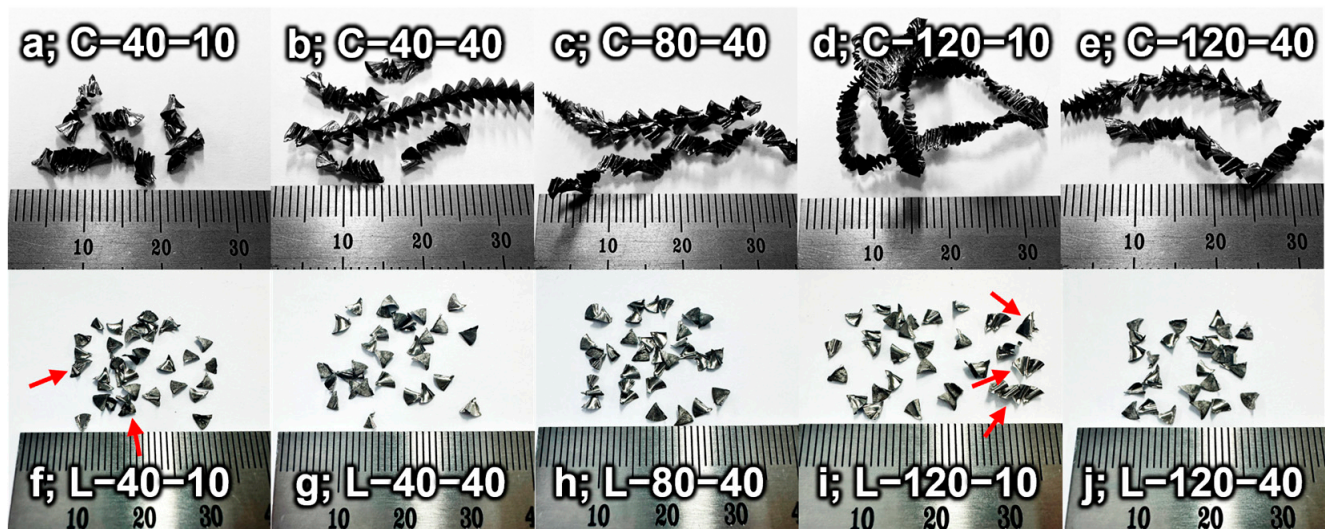


Figure 4. Chip morphology dependent on machining process (CD and LF-VAD) and coolant pressure (red arrows indicate areas where parts are attached and not completely separated).

In this study, the vibration device (PM 4225, MITIS, Bouguenais, France) utilized for LF-VAD machining incorporates a mechanical cam structure, resulting in a fixed vibration frequency of 2.5 times per one rotation. Consistent with previous research findings, machining was conducted at a feed rate of 0.08 mm/rev, recognized as the most effective for chip segmentation and overall machining efficiency [27]. Given the fixed nature of the vibration frequency and feed rate per revolution, substantial variations in the chip formation mechanism due to machining conditions in LF-VAD are not anticipated. Consequently, no significant difference in the shape of the chips was observed across conditions machined at cutting speeds ranging from 40 m/s to 120 m/s.

Nevertheless, variations in cooling conditions, such as cutting fluid pressure and cutting speed, introduce slight differences in the shape of chips discharged in LF-VAD. Firstly, in processes with a cutting fluid pressure set to 10 bar (Figure 4f,i), chip segmentation occurred normally; however, due to insufficient cutting fluid pressure, elevated temperature, and adhesion wear, complete fragmentation did not occur. While numerical analysis is impeded by constraints in the machining process and chip collection (attributed to the cutting fluid), an observed phenomenon is the occasional inadequate cutting of chips, causing them to stick together more frequently. The phenomenon can be observed in Figure 4, indicated by the red arrows for the L-40-10 and L-120-10 conditions. Conversely, in processes with a high cutting fluid pressure of 40 bar (Figure 4g,h,j), chip segmentation and fragmentation occurred smoothly. This suggests that low cutting fluid pressure in LF-VAD machining hampers chip segmentation, potentially leading to chip clogging in hole machining processes. This underscores the importance of maintaining an appropriate cutting fluid pressure in LF-VAD machining.

The impact of low coolant pressure on temperature variation in the LF-VAD process is elucidated through the analysis of chip phase morphology in Figure 5, specifically examining the L-120-10 and L-120-40 conditions. In the LF-VAD process, chips segment; however, under the L-120-10 condition where perfect separation is not achieved, the grain size is notably larger compared with that under the L-120-40 condition. The elevated temperature during material cutting is subsequently reduced through internal coolant and

chip expulsion. Under the L-120-40 condition, efficient chip separation and expulsion, facilitated by sufficient coolant pressure, result in a rapid temperature decrease. The elevated temperature causes chips with larger grain sizes to rapidly cool down, transforming into smaller-grain chips. Conversely, under the L-120-10 condition where adequate heat dissipation is lacking, chips with larger grain sizes persist due to a relatively slow temperature decrease. This interpretation explains the observed phenomenon of chip adhesion, underscoring the critical role of an appropriate cooling mechanism.

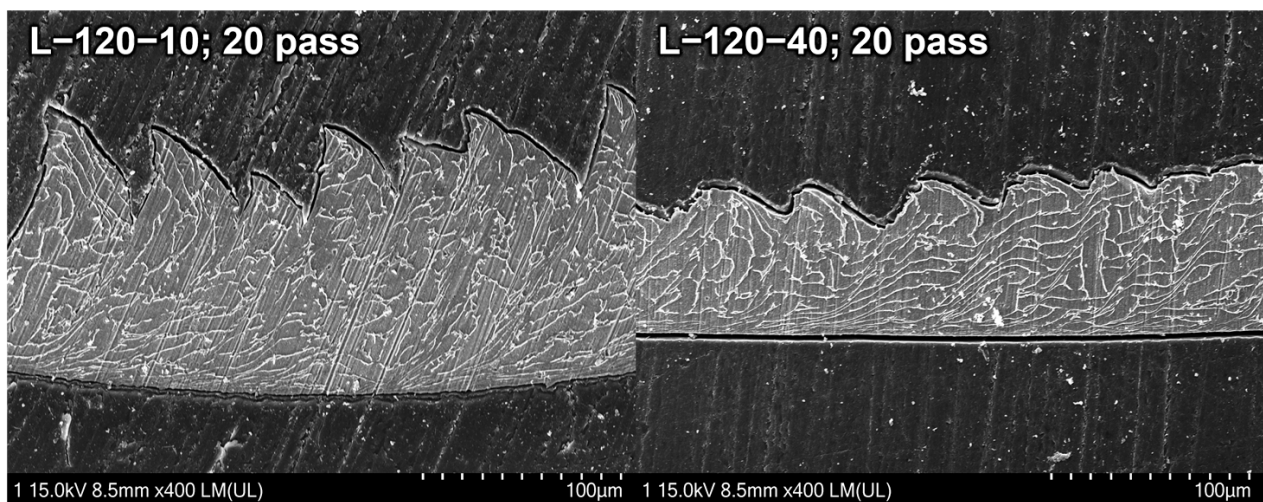


Figure 5. Comparison of phase morphology of Ti-6Al-4V ELI chips under different coolant pressures. Under the L-120-10 condition, a larger grain size is observed compared to the L-120-40 condition, indicating the challenge of insufficient cooling.

In contrast, in the CD process, where there are no physical devices such as LF-VAD to induce chip segmentation, deviations tend to become relatively larger with changes in the cutting speed. Titanium chips in the CD process exhibit features such as sawtooth edges, localized shearing, discontinuity, periodicity, and a splintered form, resulting in shapes such as spiral-cone shapes or folded ribbons.

When comparing chip morphology at the same cutting fluid pressure of 40 bar and varying cutting speeds in the CD process (Figure 4b,c,e), at a cutting speed of 40 m/s, a stable spiral-cone shape is observed with certain instances of folded ribbon chips (Figure 4b). As the cutting speed increases to 80 m/s, a transitional phase is noted where the spiral-cone-shaped chips are not smoothly ejected but rather compressed into folded long chips (Figure 4c). At a cutting speed of 120 m/s, a fully formed folded long ribbon chip is observed (Figure 4d). The phenomenon of folded ribbon chip formation intensifies as chip ejection resistance increases, particularly when the cutting fluid pressure is reduced to 10 bar. Unlike the stable formation of spiral chips observed under the C-40-40 condition, the C-40-10 condition exhibits the formation of folded ribbon chips as the cutting fluid pressure decreases. Similarly, when experimenting with higher cutting speeds and lower cutting fluid pressure, as under the C-120-10 condition, even longer folded ribbon chips are generated.

As chip ejection resistance increases, the formation of folded long ribbon chips can lead to several issues during drilling, including increased thrust force, accelerated tool wear, and a deterioration in hole quality. Even the ideal chip morphology, i.e., the spiral-cone shape obtained through the CD process can be affected by scratches generated during chip transport from the cutting region to the exit, impacting the surface quality around the hole. Based on the results regarding chip morphology, LF-VAD offers clear advantages compared with CD. In LF-VAD machining, although complete separation of segmented chips may not occur as the cutting speed increases, the chip segmentation process is effectively managed

through a mechanical mechanism, and optimization can be achieved by adjusting the cutting speed.

In conclusion, LF-VAD effectively achieves chip segmentation under most conditions. However, it was observed that under low coolant pressure conditions (10 bar), complete segmentation of chips does not occur. The insufficient segmentation of chips under such conditions appears to be associated with the elevated temperature resulting from the low cutting fluid pressure, as evidenced by the analysis of chip morphology.

3.3. Tool Wear

Here, trends in tool wear are analyzed after machining the Ti-6Al-4V ELI material with a thickness of 30 mm for 20 passes. Tool wear can manifest in various forms, including chisel edge wear, flank wear, and chipping wear. Figure 6 illustrates the wear on the chisel edge area for each cutting condition. The analysis reveals clear differences in chisel edge wear based on the machining method (CD and LF-VAD) and machining conditions (coolant pressure and cutting speed). However, unusual trends are scarcely observed in flute wear, chipping wear, crater wear, and other wear types.

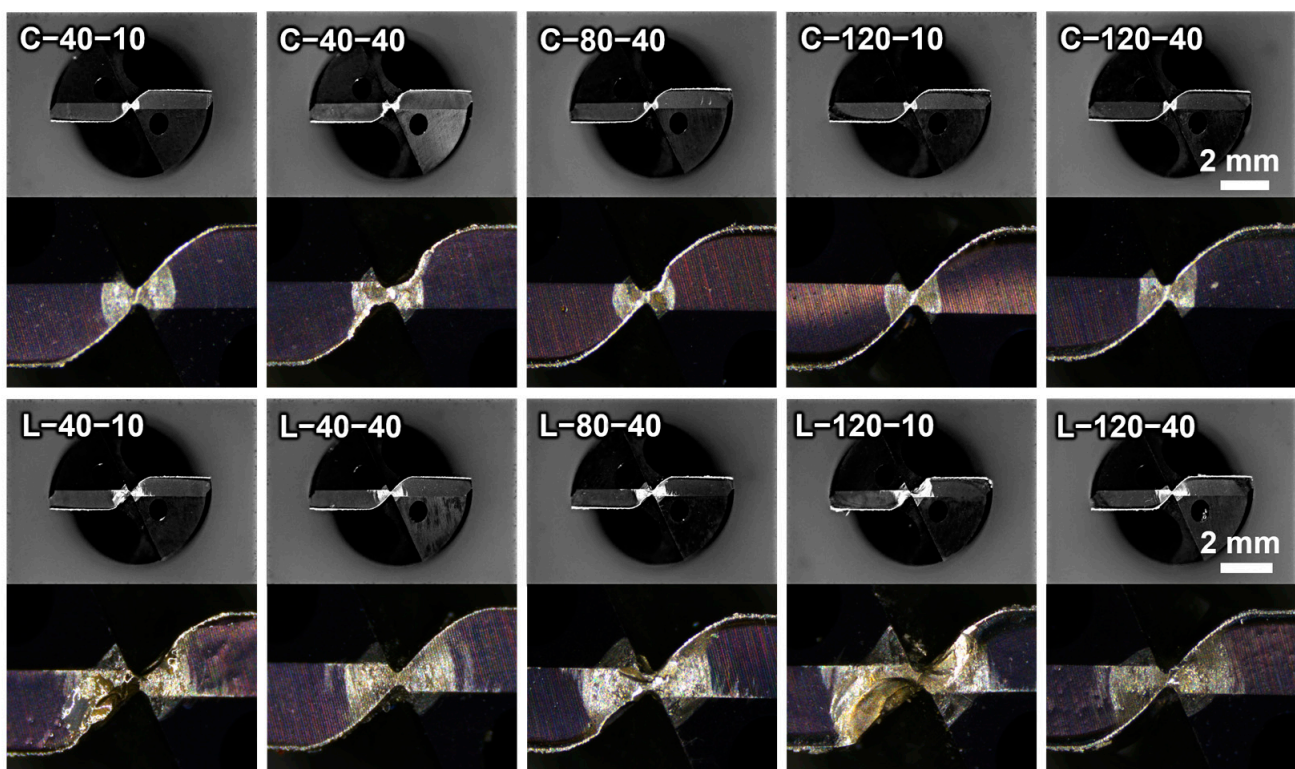


Figure 6. Image of the overall tool wear pattern and enlarged image of the chisel edge area.

Comparing tool wear in the chisel edge area between LF-VAD and CD processes conducted at the same cutting speed and cutting fluid pressure, it becomes evident that tool wear is significantly higher in LF-VAD for all conditions. In LF-VAD processing, tool wear in this area is attributed to the strong compressive forces applied periodically due to the axial vibration, a characteristic of the LF-VAD process. During this process, the high chemical affinity between the titanium alloy and the tool, coupled with the temperature increase resulting from compression, leads to increased adhesion between the material and the tool, promoting wear [28]. This wear is even more pronounced under conditions with a coolant pressure of 10 bar.

In conclusion, from the perspective of tool wear, LF-VAD performs less favorably than CD. While LF-VAD effectively induces chip removal, reducing cutting resistance, and can

reduce thrust forces (RMS) with appropriate cooling conditions, its unique cutting method exerts more force on the tool, thereby accelerating wear.

3.4. Burr Height and Surface Roughness

The surface quality of a hole is defined by parameters such as burr formation and surface roughness. Among these, burr formation is a common issue during the drilling process and occurs due to the plastic deformation of the material. As the tool approaches the hole's exit, the material undergoes plastic deformation. If it cannot withstand this deformation, it can lead to crack initiation at the hole's edge or extrusion of material outward, resulting in burr formation. Typically, burrs are formed at the entrance and exit of the hole, significantly affecting dimensional accuracy. While entrance burrs are usually small and can be easily removed during the chamfering process, exit burrs pose a more significant challenge in terms of removal. Residual exit burrs create stress concentrations, serving as initiation points for fatigue failure and corrosion, ultimately reducing the lifespan of mechanical components. Moreover, the process of removing these burrs contributes to manufacturing costs that cannot be overlooked. This, in turn, increases machining time and reduces production efficiency. Considering the impact on product quality, lifespan, and production costs, it is crucial to implement measures to suppress burr formation during the machining process.

Figure 7 illustrates a graph depicting the variation in burr size based on cutting speed and machining processes. Detailed images of the measured results for burrs are presented in Figure S1. In the preceding analysis, LF-VAD processes with low cutting fluid pressure (10 bar) exhibited a sharp increase in thrust forces and wear levels as the number of passes increased. Therefore, these conditions were excluded for the analysis determining hole quality. Burr analysis involved measuring the length at two points for each condition and calculating the average value for analysis. The results indicate that LF-VAD conditions recorded burr sizes equal to or smaller than CD conditions under all cutting speed conditions. Under the L-120-40 condition, the average burr size was 109.5 μm , approximately 40% smaller than the 183 μm measured under the C-120-40 condition. Similarly, the average burr size under the L-40-40 condition was 79 μm , approximately 44% smaller than the 141.5 μm measured under the C-40-40 condition. At a cutting speed of 80 m/s, almost similar burr sizes were observed, with the L-80-40 condition showing slightly smaller burrs. This indicates that LF-VAD is effective in suppressing burr formation in the drilling of Ti-6Al-4V ELI material for most conditions. However, when comparing LF-VAD processes alone, it is evident that burr size increases linearly with increasing cutting speed. This trend is attributed to the machining temperature. High cutting speeds elevate the machining temperature, accumulating a significant amount of heat in the material that increases its ductility. Increased ductility enhances material flowability, allowing for machining with lower thrust forces. However, at the exit point, the tool pushes out the more ductile material, affecting burr size significantly. Through this comparison, it is confirmed that LF-VAD is a superior machining method in terms of burr size. Additionally, this burr analysis also confirms that LF-VAD machining operates at lower temperatures compared with CD machining.

Surface roughness is another important parameter in determining hole quality, and Figure 8 presents the variation in surface roughness with cutting speed and machining process. In addition, more detailed data on surface roughness measurements can be found in Table S1. The graph illustrates that holes machined by the LF-VAD process exhibit lower surface roughness (L-40-40, L-80-40). This is because LF-VAD machining effectively suppresses the scratching of the hole's interior surface during the exit of chips along the tool's flute, unlike in the CD process where continuous chips are expelled, causing scratching. However, for conditions processed at a cutting speed of 120 m/s, it can be observed that the surface roughness for LF-VAD-machined conditions is slightly higher. This can be attributed to the earlier chip analysis that showed that chips under the L-120-40 condition did not completely separate.

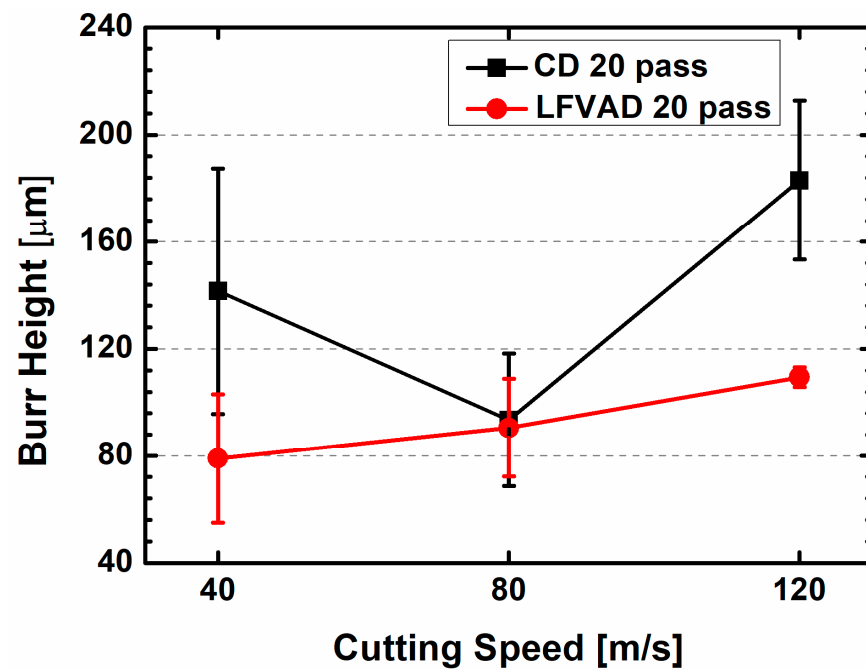


Figure 7. Comparison of burr height at 20 passes according to processing conditions and cutting speeds.

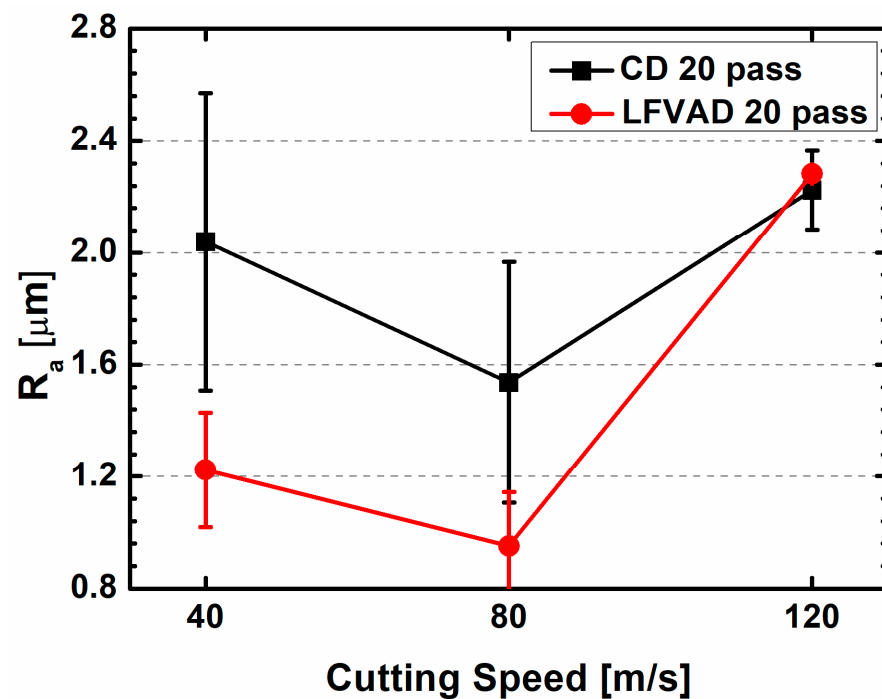


Figure 8. Comparison of surface roughness (R_a) at 20 passes according to processing conditions and cutting speeds. Comparison of burr height at 20 passes according to processing conditions and cutting speeds.

The size of the burr and surface roughness are critical parameters that determine product quality, and LF-VAD machining conditions set under appropriate parameters (in this study, the L-80-40 condition) appear to provide a smoother and more uniform surface compared with CD, primarily due to lower cutting temperatures and superior chip evacuation characteristics.

In conclusion, it can be confirmed that machining using LF-VAD can effectively reduce the surface roughness and burr size on the inner hole surface. However, the optimal cutting

speed varies depending on the priority. Surface roughness on the inner hole surface can be effectively reduced at cutting speeds of 40 m/s and 80 m/s, but statistically significant results are not found at 120 m/s. On the other hand, burr height shows the most significant reduction at 40 m/s and a substantial decrease at 120 m/s, but there is not a difference observed at 80 m/s. These results indicate the importance of using appropriate parameters based on priorities when employing LF-VAD in actual machining.

3.5. Residual Stress

Residual stress is a crucial factor influencing crack generation and fatigue behavior. Generally, compressive residual stress does not significantly contribute to destruction. However, tensile residual stress on the surface can promote corrosion and initiate cracks under stress, thereby reducing fatigue life. Therefore, managing residual stress induced by machining is crucial for improving the quality of machined parts.

In this study, the influence of LFVAD on residual stress was examined in comparison to the CD process. Figures 9 and S2 illustrates how residual stress levels change with cutting process and cutting speed. Residual stress analysis excluded the condition of cutting fluid pressure at 10 bar, as it exhibited substantial tool wear with an increasing number of passes. Measurements reveal a consistent trend, regardless of the machining conditions in both CD and LFVAD processes. As cutting speed increased, residual stress tended to shift towards tensile stress. However, it is worth noting a significant difference. In CD process conditions, with increasing cutting speed, residual stress also increased, resulting in tensile residual stress. This was evident in the C-120-40 condition, where 113 MPa of tensile residual stress was observed. In contrast, under LFVAD process conditions, even at a cutting speed of 120 m/s in the L-120-40 condition, compressive residual stress of -211 MPa was observed. The L-80-40 condition, which exhibited the most favorable trends in hole quality, recorded an even higher compressive residual stress of -445 MPa. These results highlight the substantial differences in residual stress profiles between CD and LFVAD processes.

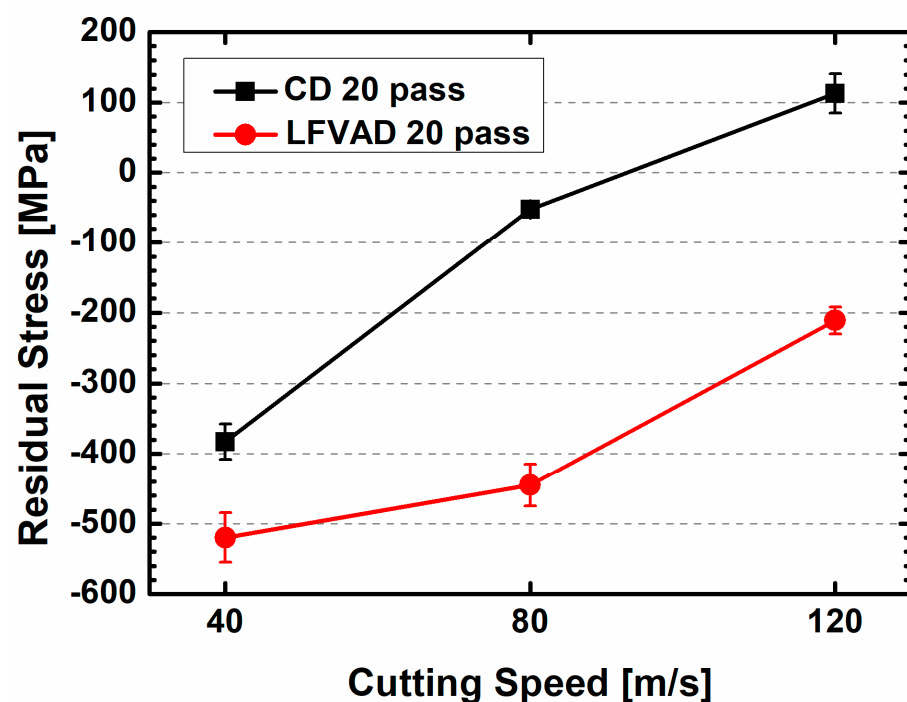


Figure 9. Comparison of residual stresses at 50 μ m depth depending on the cutting process and cutting speed.

Drilled holes play a vital role in the assembly of machine parts, such as bolts and rivets, where substantial stresses are encountered in real machinery applications. The presence of compressive residual stresses, when subjected to these applied stresses, serves as a pre-

ventive measure against crack formation. This inhibition of corrosion and stress corrosion cracking significantly enhances the fatigue life of components and the overall system.

4. Conclusions

This study conducted a comprehensive analysis of the differences between LF-VAD and CD processes, focusing on various aspects of machining. The key findings of the analysis are as follows:

- LF-VAD exhibits a higher maximum thrust force than CD due to its unique machining mechanism, but the RMS (root mean square) thrust force is lower. Increasing coolant pressure has the effect of suppressing the increase in thrust force in LF-VAD.
- To achieve effective chip segmentation in LF-VAD, the use of sufficient coolant pressure and not excessively high cutting speed is required.
- LF-VAD shows a weakness in tool wear compared to CD. The use of low coolant pressure accelerates wear in the LF-VAD process.
- LF-VAD can achieve lower surface roughness and burr size and induce higher comprehensive residual stress depending on machining conditions. These achievements enhance the mechanical stability of the machined hole and ultimately improve the product's lifespan.

Overall, LF-VAD has the disadvantage of potentially worsening tool wear. However, its advantages, such as optimizing chip segmentation, surface roughness, residual stress, and burr size under appropriate machining conditions, make it applicable to high-value-added industries where product quality and lifespan are crucial.

Supplementary Materials: The following supporting information can be downloaded at: <https://www.mdpi.com/article/10.3390/jmmp7060209/s1>, Figure S1: OM (Optical Microscope) images displaying burrs after drilling processing; Figure S2: The detailed residual stress results measured under each condition; Table S1: The detailed surface roughness results measured under each condition.

Author Contributions: Conceptualization, D.M.K.; Validation, J.H.H.; Formal analysis, J.-H.C.; Investigation, J.-H.C. and J.H.H.; Resources, J.K.; Writing—original draft, J.-H.C.; Writing—review & editing, J.H.H.; Supervision, J.K. and D.M.K.; Project administration, J.K. and D.M.K.; Funding acquisition, J.K. and D.M.K. All authors have read and agreed to the published version of the manuscript.

Funding: This research work was supported by the Basic Science Research Program through the National Research Foundation of Korea (NRF) funded by the Ministry of Education (2021R111A3045191) and the development of holonic manufacturing system for future industrial environment funded by the Korea Institute of Industrial Technology (KITECH EO-23-0006).

Data Availability Statement: Data are contained within the article and supplementary materials.

Conflicts of Interest: The authors declare no conflict of interest.

References

1. Gurrappa, I.; Reddy, D.V. Characterisation of Titanium Alloy, IMI-834 for Corrosion Resistance under Different Environmental Conditions. *J. Alloys Compd.* **2005**, *390*, 270–274. [\[CrossRef\]](#)
2. Lütjering, G. Influence of Processing on Microstructure and Mechanical Properties of (A+ β) Titanium Alloys. *Mater. Sci. Eng. A* **1998**, *243*, 32–45. [\[CrossRef\]](#)
3. Boyer, R.R. An Overview on the Use of Titanium in the Aerospace Industry. *Mater. Sci. Eng. A* **1996**, *213*, 103–114. [\[CrossRef\]](#)
4. Nikiel, P.; Wróbel, M.; Szczepanik, S.; Stepień, M.; Wierzbowski, K.; Baczmański, A. Microstructure and Mechanical Properties of Titanium Grade 23 Produced by Selective Laser Melting. *Arch. Civ. Mech. Eng.* **2021**, *21*, 152. [\[CrossRef\]](#)
5. Ezugwu, E.O.; Wang, Z.M. Titanium Alloys and Their Machinability—A Review. *J. Mater. Process. Technol.* **1997**, *68*, 262–274. [\[CrossRef\]](#)
6. Schutz, R.W.; Baxter, C.F.; Boster, P.L.; Fores, F.H. Applying Titanium Alloys in Drilling and Offshore Production Systems. *JOM* **2001**, *53*, 33–35. [\[CrossRef\]](#)
7. Gurrappa, I. Characterization of Titanium Alloy Ti-6Al-4V for Chemical, Marine and Industrial Applications. *Mater. Charact.* **2003**, *51*, 131–139. [\[CrossRef\]](#)

8. Okazaki, Y.; Ito, Y.; Kyo, K.; Tateishi, T. Corrosion Resistance and Corrosion Fatigue Strength of New Titanium Alloys for Medical Implants without V and Al. *Mater. Sci. Eng. A* **1996**, *213*, 138–147. [\[CrossRef\]](#)
9. Follansbee, P.S.; Gray, G.T. An Analysis of the Low Temperature, Low and High Strain-Rate Deformation of Ti–6Al–4V. *Met. Trans. A* **1989**, *20*, 863–874. [\[CrossRef\]](#)
10. Pramanik, A.; Islam, M.N.; Basak, A.; Littlefair, G. Machining and Tool Wear Mechanisms during Machining Titanium Alloys. *Adv. Mater. Res.* **2013**, *651*, 338–343. [\[CrossRef\]](#)
11. Pramanik, A. Problems and Solutions in Machining of Titanium Alloys. *Int. J. Adv. Manuf. Technol.* **2014**, *70*, 919–928. [\[CrossRef\]](#)
12. Chichili, D.R.; Ramesh, K.T.; Hemker, K.J. The High-Strain-Rate Response of Alpha-Titanium: Experiments, Deformation Mechanisms and Modeling. *Acta Mater.* **1998**, *46*, 1025–1043. [\[CrossRef\]](#)
13. Maňkova, I.; Vrabel, M.; Kandrác, L. Evaluation of Chip Morphology When Drilling Titanium Alloy. *Cut. Tools Technol. Syst.* **2019**, *91*, 134–142. [\[CrossRef\]](#)
14. Sharif, S.; Rahim, E.A. Performance of Coated- and Uncoated-Carbide Tools When Drilling Titanium Alloy—Ti–6Al4V. *J. Mater. Process. Technol.* **2007**, *185*, 72–76. [\[CrossRef\]](#)
15. Graves, A.; Teike, M.; Norg, S.; Crawforth, P.; Jackson, M. The Effect of Titanium Alloy Composition and Tool Coating on Drilling Machinability. *MATEC Web Conf.* **2020**, *321*, 13002. [\[CrossRef\]](#)
16. Shokrani, A.; Dhokia, V.; Newman, S.T. Investigation of the Effects of Cryogenic Machining on Surface Integrity in CNC End Milling of Ti–6Al–4V Titanium Alloy. *J. Manuf. Process.* **2016**, *21*, 172–179. [\[CrossRef\]](#)
17. Shokrani, A.; Dhokia, V.; Muñoz-Escalona, P.; Newman, S.T. State-of-the-Art Cryogenic Machining and Processing. *Int. J. Comput. Integr. Manuf.* **2013**, *26*, 616–648. [\[CrossRef\]](#)
18. Shokrani, A.; Newman, S.T. A New Cutting Tool Design for Cryogenic Machining of Ti–6Al–4V Titanium Alloy. *Materials* **2019**, *12*, 477. [\[CrossRef\]](#)
19. Hall, S.; Loukaides, E.; Newman, S.T.; Shokrani, A. Computational and Experimental Investigation of Cutting Tool Geometry in Machining Titanium Ti–6Al–4V. *Procedia CIRP* **2019**, *86*, 139–144. [\[CrossRef\]](#)
20. Wang, T.Q.; Liu, Z.F.; Qiu, Y.Y.; Feng, Y.Z.; Han, X.L. Removal Mechanism of Titanium Alloy Material in Ultrasound Vibration Drilling. *Mater. Sci. Forum* **2020**, *993*, 3–11. [\[CrossRef\]](#)
21. Hussein, R.; Sadek, A.; Elbestawi, M.A.; Attia, M.H. Surface and Microstructure Characterization of Low-Frequency Vibration-Assisted Drilling of Ti6Al4V. *Int. J. Adv. Manuf. Technol.* **2019**, *103*, 1443–1457. [\[CrossRef\]](#)
22. Sadek, A.; Attia, M.H.; Meshreki, M.; Shi, B. Characterization and Optimization of Vibration-Assisted Drilling of Fibre Reinforced Epoxy Laminates. *CIRP Ann. Manuf. Technol.* **2013**, *62*, 91–94. [\[CrossRef\]](#)
23. Wang, X.; Wang, L.J.; Tao, J.P. Investigation on Thrust in Vibration Drilling of Fiber-Reinforced Plastics. *J. Mater. Process. Technol.* **2004**, *148*, 239–244. [\[CrossRef\]](#)
24. Debnath, K.; Singh, I. Low-Frequency Modulation-Assisted Drilling of Carbon-Epoxy Composite Laminates. *J. Manuf. Process.* **2017**, *25*, 262–273. [\[CrossRef\]](#)
25. Okamura, K.; Sasahara, H.; Segawa, T.; Tsutsumi, M. Low-Frequency Vibration Drilling of Titanium Alloy. *JSME Int. J. Ser. C Mech. Syst. Mach. Elements Manuf.* **2006**, *49*, 76–82. [\[CrossRef\]](#)
26. Yang, H.; Ding, W.; Chen, Y.; Laporte, S.; Xu, J.; Fu, Y. Drilling Force Model for Forced Low Frequency Vibration Assisted Drilling of Ti–6Al–4V Titanium Alloy. *Int. J. Mach. Tools Manuf.* **2019**, *146*, 103438. [\[CrossRef\]](#)
27. Xu, J.; Li, C.; Chen, M.; Ren, F. A Comparison between Vibration Assisted and Conventional Drilling of CFRP/Ti6Al4V Stacks. *Mater. Manuf. Process.* **2019**, *34*, 1182–1193. [\[CrossRef\]](#)
28. Yan, C.; Chen, Y.; Yang, H.; Qian, N.; Chen, Y.; Guo, N. Machining Performance of PCD Drill in Low-Frequency Vibration-Assisted Drilling of CFRP/Ti6Al4V Stack: With Special Emphasis on the Plowing Behavior. *Int. J. Adv. Manuf. Technol.* **2021**, *116*, 2269–2283. [\[CrossRef\]](#)
29. Yang, H.; Chen, Y.; Xu, J.; Ladonne, M.; Lonfrier, J.; Fu, Y. Tool Wear Mechanism in Low-Frequency Vibration-Assisted Drilling of CFRP/Ti Stacks and Its Individual Layer. *Int. J. Adv. Manuf. Technol.* **2019**, *104*, 2539–2551. [\[CrossRef\]](#)
30. Chang, S.S.F.; Bone, G.M. Thrust Force Model for Vibration-Assisted Drilling of Aluminum 6061-T6. *Int. J. Mach. Tools Manuf.* **2009**, *49*, 1070–1076. [\[CrossRef\]](#)
31. Brinksmeier, E.; Pekat, O.; Rentsch, R. Quantitative Analysis of Chip Extraction in Drilling of Ti6Al4V. *CIRP Ann. Manuf. Technol.* **2015**, *64*, 93–96. [\[CrossRef\]](#)
32. Li, S.; Peng, H.; Ding, C.; Tang, H.; Liu, C. Deep-Hole Axis Deviation Mechanism of Weak Stiffness Small-Diameter Single-Lip Tool in Low-Frequency Vibration-Assisted Drilling. *Int. J. Adv. Manuf. Technol.* **2023**, *124*, 2719–2737. [\[CrossRef\]](#)
33. Matweb Home Page. Available online: <https://www.matweb.com/search/MaterialGroupSearch.aspx> (accessed on 10 October 2023).

Disclaimer/Publisher’s Note: The statements, opinions and data contained in all publications are solely those of the individual author(s) and contributor(s) and not of MDPI and/or the editor(s). MDPI and/or the editor(s) disclaim responsibility for any injury to people or property resulting from any ideas, methods, instructions or products referred to in the content.